



# Determination of rock mass strength parameters for use in local-scale seismic landslide hazard zonation, Roudbar quadrangle, Iran

M. E. Mirabedini<sup>1</sup> · E. Haghshenas<sup>2</sup> · N. Ganjian<sup>1</sup>

Received: 6 March 2022 / Revised: 17 May 2022 / Accepted: 19 May 2022 / Published online: 8 July 2022  
© The Author(s), under exclusive licence to Korean Spatial Information Society 2022

**Abstract** The aim is to identify and assessment of the shear strength parameters ( $\phi$  and  $c$ ) of the geological formation in the Roudbar quadrangle at a regional scale, to be used in seismic landslide hazard or susceptibility zonation. In this study, the earthquake-induced landslide inventory map following Roudbar-Manjil Earthquake was prepared. The geotechnical data of these studies, as well as findings from local consultants and construction projects, were collected as well. The shear strength parameters of each formation were then assessed by employing the geotechnical strength index classification system introduced. We illustrate the use of Newmark's sliding block and Gibson's applicable definition to evaluate strength parameter data. Newmark's displacement method and Jibson's applicable definition were employed to validate strength parameter data for slope static stability analysis. Slope stability analysis was modeled in a GIS environment using a digital elevation map and the normalized difference moisture index. The normalized difference moisture index was used to assess moisture content derived from Landsat spectral bands 4 and 5. Finally, the

pseudo-static back-analysis of one sample landslide was performed to validate the strength parameters. The study provides necessary data for rapidly creating a map of earthquake-triggered landslides.

**Keywords** Back-analysis · Formation · GSI · NDMI · Strength parameters

## 1 Introduction

In general, earthquake-triggered landslides can cause severe economic, human, and environmental losses, especially in mountainous areas [1, 2]. Landslides accounted for nearly 40% of global natural hazards during 1900–2014 [3]. Accordingly, identifying the region's susceptibility is highly important to avoid landslide damage or reduce consequent losses. Different methods have been developed on local, regional, and national or global scales [4, 5] and have broadly been classified into qualitative and quantitative types [6, 7]. The group of the quantitative methods includes statistical methods such as frequency ratio or logistic regression [8, 9], machine learning methods, e.g., random forest [10, 11], artificial neural networks [12, 13] or support vector machines [14, 15] and Analytical methods (Newmark Displacement method). Quantitative methods can be divided into statistical, machine learning/data mining, and deterministic methods [16, 17]. Newmark (1965) proposed a single rigid block method for analyzing the deformation of embankments and dams caused by earthquake shaking, and Wilson and Keefer (1983) applied it for assessing the stability of natural slopes under earthquake shaking [18, 19]. Since the last decade, using Newmark's displacement method [20, 21] accompanied by the Geographic Information System (GIS) has become a functional deterministic

**Supplementary Information** The online version contains supplementary material available at <https://doi.org/10.1007/s41324-022-00455-4>.

✉ E. Haghshenas  
haghshen@iiees.ac.ir; arminesaheli@gmail.com

M. E. Mirabedini  
mirabedinime3@gmail.com

N. Ganjian  
navidganjian@yahoo.com

<sup>1</sup> Department of Civil Engineering, Science and Research Branch, Islamic Azad University, Tehran, Iran

<sup>2</sup> International Institute of Earthquake Engineering and Seismology (IIEES), Tehran, Iran

approach to prepare the seismic landslide hazard map [22, 23]. Landslide hazard zonation based on Newark's permanent displacement analysis is a valuable method for creating susceptibility or hazard maps [24]. This model treats the slope as a rigid body, and the accumulated permanent displacement is calculated throughout the analysis process. Jibson et al. [25] developed a method for producing a digital probabilistic seismic landslide hazard map using Newark's method. In this model, Permanent displacement of the landslide occurs when the seismic acceleration exceeds a critical value, and critical acceleration is a simple function of the static factor of safety. The static stability coefficient of slopes directly depends on the shear strength parameters of the jointed rock masses, cohesive ( $c$ ), friction angle ( $\phi$ ), and the determining shear strength parameters of jointed rock masses. Laboratory and in situ tests, rock classification systems, and empirical criteria are different methods for estimating the shear strength parameters of rock masses. Nonetheless, laboratory and in situ tests are unreliable because of the associated sample effects and fracture systems [26, 27]. It is generally accepted that the obtained shear strength parameters from the back-analysis of slope failure are more reliable than those from laboratory and in situ testing [28]. On the other hand, it has been recently accepted that the empirical failure criterion of Hoek and Brown [64] and geotechnical strength index (GSI) classification system could be valuable approaches for estimating the rock mass strength and deformation parameters [29]. The Newmark sliding block method has been used to assess earthquake-triggered landslides in Los Angeles, California [30], Roudbar, Iran [31], Greece [32], Wenchuan, China [33], Longmenshan, China [34] and Lushan, China [35]. In Iran, after The Roudbar-Manjil earthquake, Mahdavifar (2006) generated a fully automatic version of a GIS-based system relying on a simplified Newmark's displacement method to provide a seismic landslide hazard zonation map immediately after the occurrence of an earthquake or susceptibility map by defining a scenario. This study was conducted in Alborz and the central areas of Iran [36]. The Roudbar-Manjil earthquake was one of the deadliest earthquakes causing extensive fatalities and damage to the area in Iran in 1990. According to [37], the earthquake occurred 30 min after midnight on June 21, 1990 (local time) in the northern province of Gilan, Iran ( $M_w = 7.3$ ). Several landslides and rock avalanches were triggered, the village of Fatalak was utterly ruined, and all 120 inhabitants were killed in this earthquake [38]. Different studies focused on the landslides in this region [39]. Hazard analysis of slopes for areas prone to earthquakes can help to prevent or reduce the damages. Newmark's displacement analysis methods are beneficial to analyze earthquake-induced landslide hazards on a regional scale. Mahdavifar (2006) generated a fully automatic version of a GIS-based system relying on a simplified Newmark's displacement method which could provide

a seismic landslide hazard zonation map immediately after an earthquake [40]. This study was conducted in Alborz and the central areas of Iran. Similarly, Mahdavifar [41] created a version of a GIS-based system that could present a map for seismic landslide hazard zonation based on a simplified version of Newmark's displacement method [42] following an earthquake. Such maps can be used in emergency response efforts and public information by the media. In this study, the Roudbar-Manjil earthquake was selected as a case study, and it was intended to estimate the shear strength parameters of the Roudbar geological quadrangle in the Alborz mountains range in Iran. Roudbar-Manjil earthquake occurred 30 min after midnight on June 21, 1990 (local time) in province Gilan of Iran ( $M_w = 7.3$ ). The research area was a 2400 km<sup>2</sup> quadrangle located at UTM zone 39S between 49° and 49° 30' longitudes, as well as 36° 15' and 37° latitudes (Fig. 1). The area tends to be humid, facing the Alborz and the Caspian Sea. Further, the region is located at a highly active seismic zone and is highly susceptible to landslides, which can be triggered by any significant earthquake in the north of Iran. It is also mountainous (from 150 to 2800 m above sea level). This study is focused on the determination of equivalent shear strength properties for slope stability analysis. In this regard, first, landslides triggered by the Roudbar-Manjil earthquake were mapped, then rock mass strength parameters were obtained based on some sources, and finally, pseudo-static back-analysis was performed. The study could successfully provide initial data on landslide hazard or susceptibility zonation.

## 2 Materials and methods

### 2.1 Study area

Here, we focus on the Roudbar area in Iran, affected by the 1990 Roudbar-Manjil earthquake, to assess shear strength parameters. Concerning ground motion, the Iranian territory

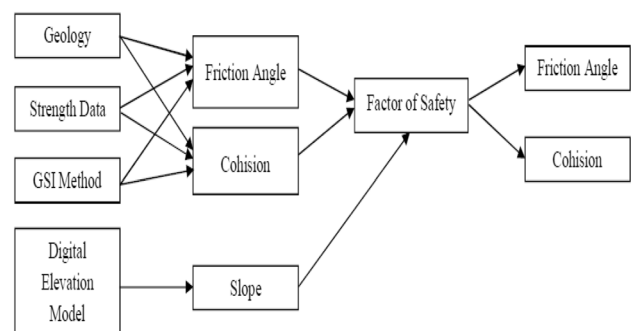


**Fig. 1** Flowchart representing steps involved in the assessment of strength parameters

can be divided into two tectonic provinces, including the Zagros zone and the Alborz and Central Iran zone.

The research area was a 2400 km<sup>2</sup> quadrangle located at UTM zone 39S between 49° and 49° 30' longitudes, as well as 36° 15' and 37° latitudes (Fig S1). The area tends to be humid, facing the Alborz and the Caspian Sea. Further, the region is located at a highly active seismic zone and is highly susceptible to landslides, which can be triggered by any significant earthquake in the north of Iran. It is also mountainous (from 150 to 2800 m above sea level).

With regard to ground motion, the Iranian territory can be divided into two tectonic provinces, including the Zagros zone and the Alborz and Central Iran zone. In the study of this region area, Roudbar geological quadrangle, located in the Alborz zone, a wide range of geological materials can be observed from the metamorphic rocks of Precambrian to Quartz sediments. In the Alborz zone, red sandstone deposits are located nearly everywhere on Infracambrian, with no changes in sedimentation and geological characteristics happening in Paleozoic. There are no Silurian and Carboniferous in this area, representing two top volume bulges at the above times. Triassic rocks are left uncomfortably overlying Permian deposits. The other may be observed at the base of Shemshak formation, namely, Jurassic [43].

Figure S2 illustrates digital geologic maps of the quadrangle forming the basis to assign material properties throughout the area. The 1:100 000-scale digital geologic maps of the Roudbar geological quadrangle are used in the current study.

## 2.2 Method

For this study, data collection, landslide inventory mapping, Google Earth imagery analysis, geographic information system (GIS)-based Newmark's displacement method and pseudo-static back-analysis model validation was applied. Furthermore, relevant data, including digital elevation model (DEM) with 10 m resolution, topographic map, historical landslide events, geological map, and shear strength parameter data were collected. These data were collected from the Central Geological Survey and mineral exploration of Iran, field survey, Google Earth imagery from the NASA. The landslide location of the study area was identified using historical records and Google Earth imagery analysis. Based on the data availability, local environmental conditions, literature, data evaluation, and local people interview, landslide inventory map was prepared using ArcGIS 10.1. Slope map was extracted from 10 m resolution of DEM, which was downloaded from the USGS website. The lithological layer map is digitized from the existing geological map of the Roudbar quadrangle sheet at a scale of 1: 100,000. The shear strength parameters database of geological formations is prepared based on Collecting compiled shear-strength and

uniaxial tests in the quadrangle, The Geological Strength Index (GSI) classification system and the judgment of several experienced geotechnical engineers.

## 2.3 Mapping landslides triggered by earthquake

Landslide inventory maps are shown to be an essential part of landslide hazard analysis. In other words, preparing landslide maps plays a crucial part in documenting the extent of landslide phenomena in a region. However, there is less than 1% landslide map of slopes [44]. Several studies have been conducted to map earthquake-triggered landslides in earthquake-prone areas, and some of them also covered the current study region [45]. However, these studies' frequently apparent differences in sources, methods, and preparation criteria. Three main steps were taken to derive the landslide map of the Roudbar-Manjil earthquake in the Roudbar quadrangle as follows:

- Studying and comparing reports, maps, and analyses performed after the Roudbar-Manjil earthquake in some parts of the region;
- Field surveying and verifying previous reports and studies;
- Comparing the results of the studies and creating an inventory of an earthquake-induced landslide in the region.

All previous studies were conducted after the earthquake and based on different methods and limitations, although the study by Mahdaviifar [46] seemed to be more realistic. Landslide inventory map was prepared by comparing the post-earthquake studies and field surveys. After comparing all previous studies and field surveys to map the inventory, post-earthquake landslides were determined, and the inventory map was prepared using ArcGIS software. Figure 3 shows a Totally 27 landslides map for the study area found based on the data of the 1990 Roudbar-Manjil earthquake (Fig. S3).

## 2.4 Newark's displacement method

Considering that land sliding is the leading cause of earthquake damages, the ability to predict earthquake-triggered landslide displacements is vital in many types of seismic-hazard or susceptibility analyses and the design of engineered slopes. Newmark's method of modeling a landslide as a rigid-plastic block sliding on an inclined plane provides an applied means of predicting approximate landslide displacements. A block's stability is affected by its weight and the friction angle and cohesion acting along a potential sliding surface, as illustrated in Fig. 4. However, the method requires knowledge of the yield or critical acceleration of

the landslide (above which permanent displacement would occur), which could be determined by the static factors of safety and landslide geometry. The critical acceleration in terms of gravity and  $a_c$  of a slope with the planar slip is determined by the Eq. (1), assuming negligible loss, in shear resistance during shaking:

$$a_c = (FS - 1) \cdot \sin a \quad (1)$$

where FS is the static factor of safety,  $a$  (thrust angle) denotes the angle between the slip direction of the center of mass and the horizontal [47] (Fig. S4). For the simplest model of an infinite slope (i.e., planar slip surface parallel to the slope), the static factor of safety is expressed as follows:

$$FS = \frac{c}{\gamma t \sin a} + \frac{\tan \phi}{\tan a} - \frac{m \gamma w \tan \phi}{\gamma \tan a} \quad (2)$$

where  $c'$ ,  $\phi'$ ,  $\gamma$ ,  $t$ , and  $m$  are the effective cohesion, the effective angle of internal friction, the material unit weight, the vertical depth of the failure surface, and the ratio of  $t$  indicating the location of the groundwater table, respectively. The slope-normal thickness is assumed to be 3 m; the most common slid depth in landslide-induced earthquakes [47].

## 2.5 Geotechnical strength parameters database

In the context of Newmark's method, Determining the rock mass strength parameters ( $\phi$  and  $c$ ) of the geological formation is necessary for calculating the safety factor of slopes.

Jibson et al. [48] determined shear strength parameters by collecting enormous direct shear test results of various local consultants using the judgment of several experienced geotechnical engineers in the region and considering all statistically stable slopes.

Fig. S5 displays a flowchart of the sequential steps involved in assessing the corresponding strength parameters of geologic formations. To be used in the seismic-landslide hazard or susceptibility zonation. The following steps were taken to produce a shear strength parameters database of geological formations is prepared based on the following steps:

- Collecting compiled shear-strength and uniaxial tests in the quadrangle and the surrounding regions;
- Using the judgment of several experienced geotechnical engineers in the region;
- Using Hoek–Brown method to estimate the strength parameters ( $\phi$  and  $c$ ) of the geological formation;
- Combining shear-strength and slope data in a factor-of-safety equation to measure the static safety factors in each grid cell based on Jibson's method.

The results of about 100 direct-shear and uniaxial tests in the study area and the surroundings were collected and obtained the experience of local geotechnical and geological engineers. There was no good agreement between these data sources, and many of the geological units contained no shear strength information. Due to the lack of shear strength data, the strength parameters of geological units were mainly clarified by applying the GSI classification system (Fig. 1).

## 2.6 GSI Estimating and equivalent shear strength parameters

The Geological Strength Index (GSI) classification system, proposed by Hoek [49] and Hoek et al. [50], has been considered as the most acceptable empirical method to estimate the rock mass strength and deformation parameters, and it can be said that there are no other suitable alternatives for it [51]. The GSI is a technique to estimate the rock mass strength in different geological conditions, using standard charts, site observation, and rock mass description. The rock mass properties can be determined considering the degree of crushing and discontinuities surfaces, indicated by roughness and alteration. Combining these two parameters provided a principal basis for describing rock mass types with diversified rock structures ranging from very tightly interlocked substantial rock fragments to heavily crushed rock masses. Based on the rock mass description, the GSI value could be estimated by the contours shown in Fig. 5 to reach a value of 0–100, representing the overall geotechnical quality of rock masses.

The GSI classification system applies to intact or heavily jointed rock masses. The Hoek–Brown failure criterion must be widely accepted for rock masses assumed to be isotropic. In other words, the behavior of the rock mass would not depend on the direction of the applied loads. Therefore, the slopes in which singular discontinuities impose failure surfaces are highly anisotropic, and the GSI system is not applicable [52]. When the failure plane passes through several zones, the GSI values require particular judgment, and the mean values may not be appropriate. A systematic study was conducted to analyze the nature and behavior of rock masses in the study area.

For this purpose, firstly, an 8-day field investigation into 320 geological stations was carried out by the leading authors and staff from the Roudbar quadrangle. Based on the mapping of the rock exposures, all the data were collected by visual chart assessments at the scale suitable for slopes. The sampling stations were identified based on good lithological exposures and the condition of slope stability. The rock slopes were selected so that they represent varied geological and slope stability conditions. The collected data included rock mass structure, rock type, joint condition, joint roughness, and hydrological condition. The GSI values were estimated qualitatively based on thorough geological visual

field observations. Figure S6 shows the route and station for collecting necessary data based on the geological map.

The rock mass was classified into four classes, i.e., blocky, very blocky, blocky disturbed, and disintegrated. The surface condition generally varies from smooth to poor, slightly weathered to highly weathered with soft clay infillings. Surface roughness data showed a wide range from rough to slickenside. From the hydrogeological point of view, all the visited slopes were dry. Three hundred-twenty locations were considered for GSI calculations, as shown in Fig. 1. The GSI evaluation showed the typical diagonal trend from top-left to bottom-right that depicted decreasing rock mass quality. It also showed that GSI values ranged from 25 to 65, i.e., from the crushed rock to almost intact rock (Figs. S7 and S8). Field photographs were taken at all slopes.

The re-evaluation of photographs revealed a structurally controlled behavior in some stations. Therefore, the GSI system was inappropriate. For this reason, the corresponding data of 26 stations were ignored, and 294 stations were considered for representing the area. Figure 3 shows the GSI measuring for two types of rock structures (Table 1).

Rock mass shear strength parameters ( $\phi$  and  $c$ ) are estimated by Roclab software. The commercial program RocLab could provide a simple and intuitive implementation of the Hoek–Brown failure criterion, allowing easily obtainable and reliable estimates of rock mass properties and visualizing the effects of changing rock mass parameters on failure envelopes. The uniaxial compressive strength  $\sigma_{ci}$  and the material constant  $m_i$  are determined by laboratory testing or estimated from published tables.

**Table 1** Field estimates of the uniaxial compressive strength of intact rock pieces

| Grade <sup>a</sup> | Term             | Uniaxial compressive strength (MPa) | Point load index (MPa) | Field estimate of strength   | Examples  |
|--------------------|------------------|-------------------------------------|------------------------|--|---|
| R6                 | Extremely strong | > 250                               | > 10                   | Specimen can only be chipped with a geological hammer  | Fresh Basalt, Chert, Diabase, Quartzite                         |
| R5                 | Very strong      | 100–250                             | 4–10                   | Specimen requires many blows of geological hammer to fracture it   | Gabbro, Gneiss, Granodiorite, Limestone, Marble, Rhyolite, Tuff |
| R4                 | Strong           | 50–100                              | 2–4                    | Specimen requires more than one blow of a geological hammer to fracture it   | Limestone, Marble, Phyllite, Sandstone, Schist, Shale           |
| R3                 | Medium strong    | 25–50                               | 1–2                    | Cannot be scarped or peeled with a pocket knife Specimen can be fractured with a single blow from a geological hammer        | Claystone, Coal, Concrete, Schist Shale, Siltstone              |
| R2                 | Weak             | 5–25                                | b                      | Can be peeled with a pocket knife with difficulty, shallow indentation made by firm blow with a point of a geological hammer | Chalk, Rocksalt, Potash   |
| R1                 | Very weak        | 1–5                                 | b                      | Crumbles under firm blows with a point of a geological hammer can be peeled by a pocket knife                                | Highly Weathered or Altered Rock                                |
| R0                 | Extremely weak   | 0.25–1                              | b                      | Indented by thumbnail  | Stiff Fault Gouge   |

<sup>a</sup>the minimum value of  $\sigma_{ci}$  and  $m_i$  was assumed to prevent the removal of the sensitive slopes

**Table 2** Values of constant  $m$  for intact rock by the rock group

| Rock name          | $m_i$  | Rock name          | $M_i$ | Rock name    | $m_i$ | Rock name   | $m_i$ |
|--------------------|--------|--------------------|-------|--------------|-------|-------------|-------|
| Conglomerate       | (22)   | Micritic limestone | 8     | Gneiss       | 33    | Diorite     | (28)  |
| Sandstone          | 19     | Gypstone           | 16    | Schists      | 4–8   | Andesite    | 19    |
| Siltstone          | 9      | Anhydrite          | 13    | Phyllites    | (10)  | Gabbro      | 27    |
| Claystone          | 4      | Marble             | 9     | Slate        | 9     | Dolerite    | (19)  |
| Greywacke          | (18)   | Hornfels           | (19)  | Granite      | 33    | Basalt      | (17)  |
| Chalk              | 7      | Quartzite          | 24    | Rhyolite     | (16)  | Norite      | 22    |
| Coal               | (8–21) | Migmatite          | 30    | Obsidian     | (19)  | Agglomerate | (20)  |
| Breccia            | 20     | Amphibolite        | 25–31 | Granodiorite | 30    | Breccia     | (18)  |
| Sparitic Limestone | 10     | Mylonites          | 6     | Dacite       | 17    | Tuff        | (15)  |



**Table 3** Shows values of initial geotechnical properties of Permian rock mass

| Age        | Geology units | Shear strength parameters based on Hoek and Brown (1980) |            | Age        | Geology units | Shear strength parameters based on Hoek and Brown (1980) |        |      |
|------------|---------------|--|------------|------------|---------------|--|--------|------|
|            |               | C (MPa)  | $\Phi$     |            |               | C (MPa)  | $\Phi$ |      |
| Quaternary | Q al          | –  | –          | Paleocene  | E 3tb         | 0.28   | 32.9   |      |
|            | Q c           | –  | –          |            | E 3tv         | 0.47   | 44.42  |      |
|            | Q tr          | –  | –          |            | E 3v          | 0.27   | 45.4   |      |
|            | Q t2          | –  | –          |            | E 2tv         | 0.47   | 43.83  |      |
|            | Q f2          | –  | –          |            | E 2t          | 0.3  | 43.6   |      |
|            | Q t1          | –  | –          |            | E 2v          | 0.29   | 28.7   |      |
|            | Q f1          | –  | –          |            | E 1tv         | 0.39   | 31.3   |      |
| Neogene    | PIQs          | 0.1  | 25.5       | E 1v       | –             |  |        |      |
|            | Pls           | 0.45   | 28.7       | E 1t       | 0.32          | 26.8   |        |      |
|            | Ng            | –  | –          | E 1t       | 0.46          | 26.63  |        |      |
|            | Ng 2          | 0.43   | 32.1       | Cretaceous | K1 c          | 0.34   | 25.11  |      |
|            | Ng 2 m        | 0.13   | 35.5       |            | K1 1          | 0.15   | 34.8   |      |
|            | Ng 2 ss1      | 0.54   | 32.6       |            | K1 2          | 0.33   | 45.91  |      |
|            | Ng 2 cs       | 0.31   | 37.02      |            | K2 sh         | 0.49   | 15.05  |      |
|            | Ng 1          | 0.29   | 37.84      |            | K2 pa c s     | 0.34   | 25.1   |      |
| Ng 1 cs    | 0.31          | 27.02  | J1 3 K 1 1 |            | 0.24          | 30   |        |      |
| Paleocene  | Mv            | 0.32   | 28.5       |            | J1 2–3        | 0.12   | 30     |      |
|            | G1            | 0.76   | 48.83      |            | Jurassic      | J mv   | 0.4    | 51.5 |
|            | G2            | 0.47   | 54.42      | T J sh ssh |               | 0.22   | 30.12  |      |
|            | EO ssh        | 0.29   | 26.6       | T J 1cs    |               | 0.8  | 35.11  |      |
|            | EO s          | 0.15   | 33.6       | T J1 s     |               | 0.4  | 27.5   |      |
|            | E tv          | 0.39   | 46.5       | T J sl     |               | 0.29   | 16.6   |      |
|            | E v           | 0.33   | 41.3       | Permian    |               | P 2–3  | 0.28   | 42.2 |
|            | E t           | 0.47   | 33.8       |            |               | P 1s   | 0.08   | 33.2 |
|            | Eta           | 0.45   | 28.1       |            |               | Ps D   | 0.05   | 34.6 |
|            | EO mt         | 0.13   | 21.1       |            |               | DEV  | Dv     | 0.48 |
| E 3tsh     | 0.23          | 39.8   |            |            |               |  |        |      |

Due to the lack of experimental data, the  $\sigma_{ci}$  of the intact rock and  $m_i$  were directly determined from Tables 2 and 3, according to suggestions by Hoek–Brown. Table 2 was the source for selecting  $\sigma_{ci}$  as well as the updated values of  $m_i$  available in Marinos and Hoek [36] (Table 3). The minimum value of  $\sigma_{ci}$  and  $m_i$  was assumed to prevent the removal of the sensitive slopes.

Unit weights were selected from published tables or similar data like Barton and Choubey [14] due to the lack of experimental data.

Another effective parameter was the disturbance factor (D), representing the degree of disturbance, ranging from 0 for undisturbed in situ rock masses to 1 for disturbed rock masses. The influence of this disturbance factor could be enormous. Sonmez and Ulusay, Cheng and Liu, Lorig and Varona, and Merrifield and Lyamin investigated the effect of the disturbance factor [12, 19]. Hoek et al. also highlighted that  $D=0.7$  and  $D=1.0$  are good

suggestions for poor and good blasting for small-scale rock slope blasting, respectively. D was assumed to be equal to unity in the current work to consider the effect of sensitive slopes.

## 2.7 Computing the static factor of safety

The static factor of safety for each grid cell must be estimated to validate the results of the obtained strength parameters, using Newmark's method and Formula 2, and as a significant constraint, the static slope model must be stable. In the following sections, each of the required steps is discussed in detail.

## 2.8 Moisture Map

The normalized difference moisture index (NDMI), which was proposed, was used to assess the moisture content.

This could be derived from Landsat spectral bands 4 and 5 and calculated using Eq. (3) as follows:

$$NDMI = [Band\ 4 - Band\ 5] / [Band\ 4 + Band\ 5] \quad (3)$$

This index contrasts the near-infrared band four and the mid-infrared band 5, which is sensitive to the reflectance of the leaf content and the absorbance of leaf moisture, respectively. The NDMI was used in this study due to the following reasons:

1. The number of rainfall stations in the study area was insufficient to provide the information layer.
2. The rainfall in different seasons is different, and the soil and rock do not absorb the precipitation in the area.

3. The amount of water absorption by the stone and soil is variable, and water absorption in the rock is highly lower compared to the soil. Using this method, NDMI images were created using Landsat spectral in 1999, close to those of the 1990 Manjil earthquake in terms of the occurrence time (Fig. 2).

Slope Map.

First, GIS software was employed, and then the 10 m digital elevation model (DEM) was produced by the 1:50 000-scale topographic map. Next, a simple algorithm of the DEM was applied to produce the slope map to compare the elevations of adjacent cells and compute the maximum slope (Fig. 3).

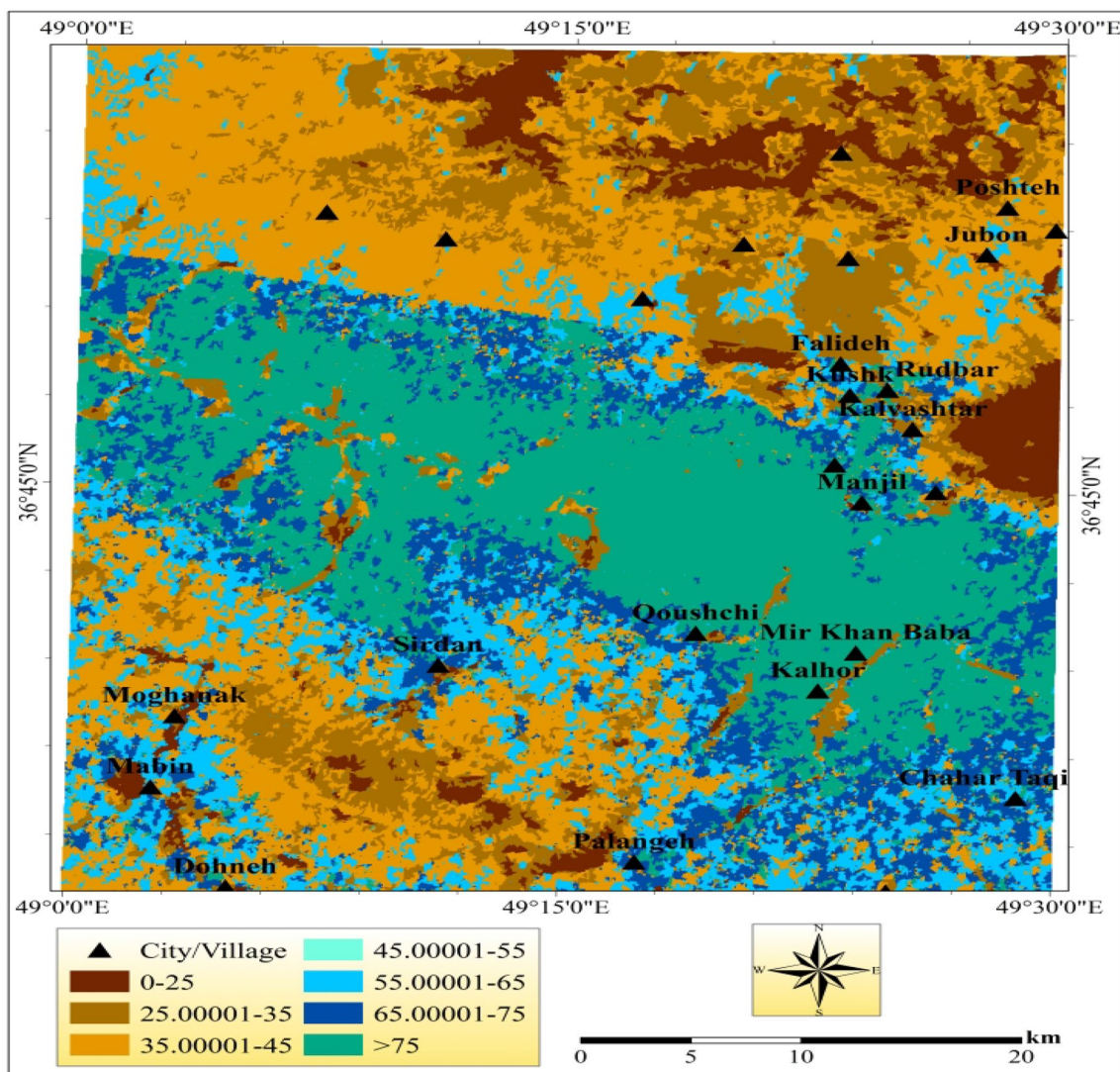
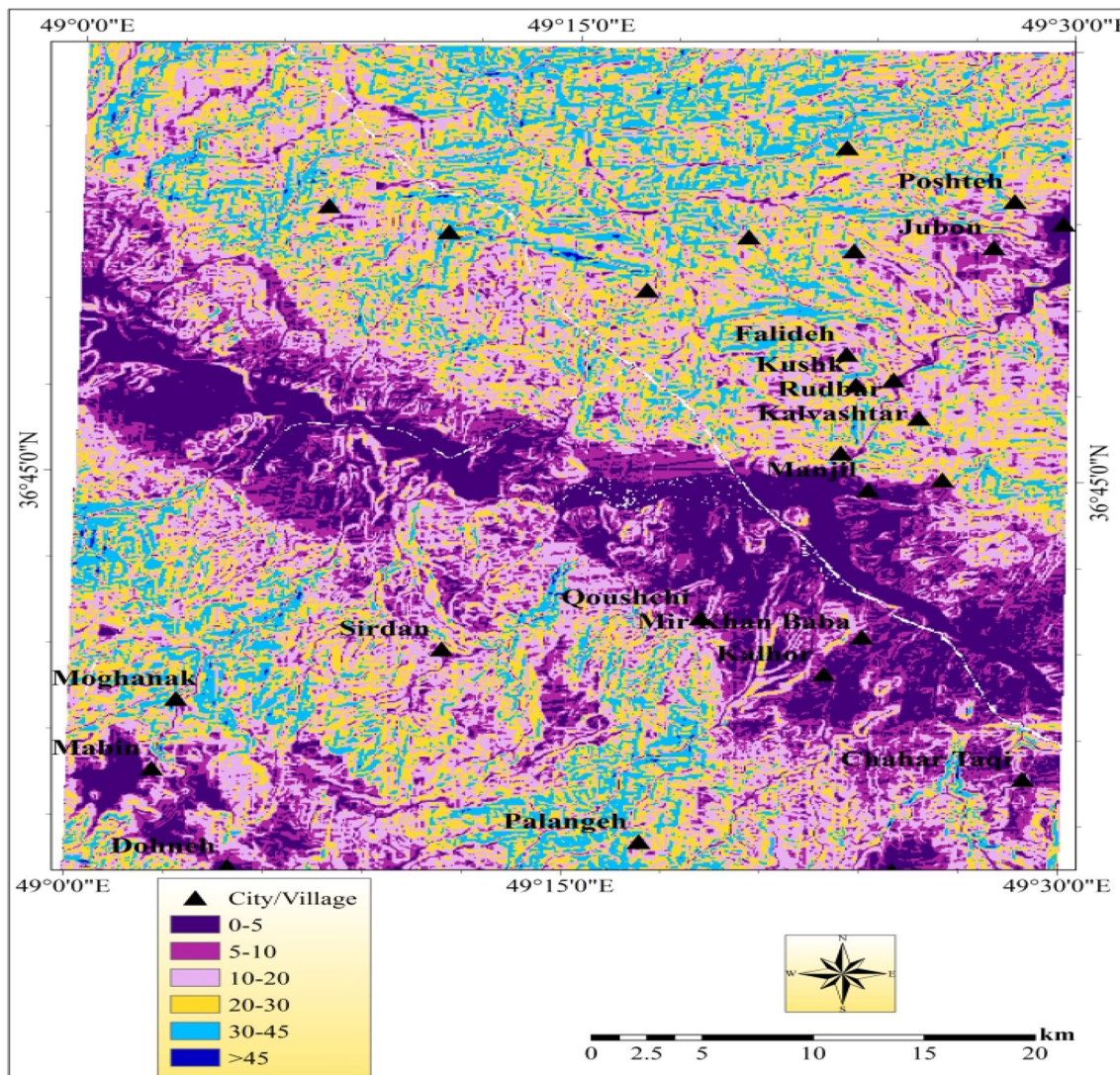


Fig. 2 Moisture content map derived by NDMI (Note. NDMI: Normalized difference moisture index.)





**Fig. 3** Slope map derived from the DEM (Note. DEM: Digital elevation map)

### 3 Result

#### 3.1 Shear-strength data

Representative shear-strength values for geologic units were selected based on the mentioned steps. This choice is due to the need to simplify the analysis and use it on geotechnical parameters' variability. For this purpose, cohesion and internal friction angle were obtained based on the field studies and Roclab software. The outputs from these values are considered as the most probable values of geotechnical parameters. These values must be considered values that have the highest probability of approaching the real ones. To determine the minimum and maximum values of geotechnical parameters (cohesion and internal friction angle) for each of the area's geological units, completely fractured rocks

and perfectly intact rocks were assumed, respectively. These values are utilized in the analysis of each unit. Figures S9 and S10 show the friction and cohesion values assigned to the geologic units.

#### 3.2 Factor-of-safety map

After preparing data layers and information, the average values of the shear strength parameters of the sources were included in the initial model iteration. For non-rock formations, the values of the peak shear strength parameters were assigned to each unit based on similar formation data and some laboratory tests. The result of combining information layers (i.e., friction angle, cohesion, and slope) in Eq. (2) as a static factor of the safety map (Fig. 4).



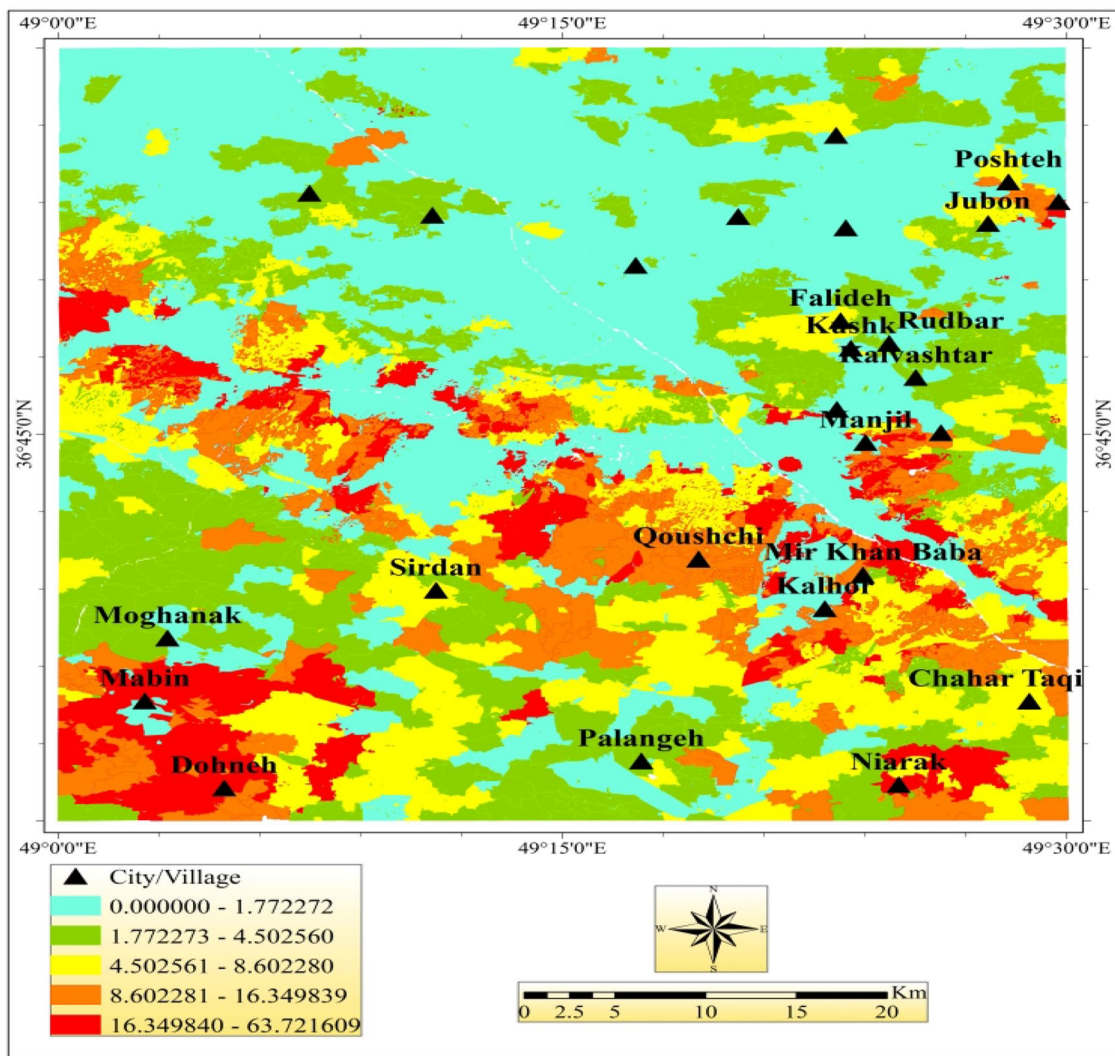


Fig. 4 Static factor-of-safety map of the part of the Roudbar quadrangle

### 3.3 Model validation

In this paper, a systematic approach of back analysis is proposed using the sensitive Pseudo-Static Back-Analysis method. The objective of this study is to identify shear strength parameters data that cause slope failure from the available information.

### 3.4 Pseudo-static back-analysis

Determining the slip surface of shear strength parameters is tricky in geotechnical engineering. The slip surface might be considered a full-scale field shear test in the soil and rock slopes. Deschamps and Yankey have extensively discussed the limitations of this approach. Back-analysis is a powerful method in understanding the failure mechanism

and determining the shear strength parameters of failed masses [94], although it is only possible for failed slopes. A successful back-analysis in rock slopes depends on the mechanism of instability.

According to Sharifzadeh et al. [40], back-analysis is an appropriate method for slopes in hard jointed rocks and slopes in heavily jointed and weak rock masses. The internal friction angle is commonly assumed in back-analysis to calculate the other ones, and the safety factor is considered equal to unity. The Mohr–coulomb linear criterion and Hoek–Brown nonlinear criterion using the specific method, developed by Sonmez et al. [41], are generally incorporated for the back-analysis. On the other hand, the limit equilibrium method is suitable for structural and non-structural failure despite all limitations.

### 3.5 Pseudo-static coefficient

The most important part of dynamic analysis is determining the seismic load acting on the slopes. The pseudo-static analysis is one of the most straightforward approaches used in earthquake engineering, and determining the seismic coefficient is the most challenging task in the pseudo-static slope stability analysis. This analysis considers the seismic load acting on the slopes through constant horizontal and vertical coefficients ( $k_h$  and  $k_v$ ), respectively. Although appropriate coefficients may play a significant role, there are no definitive rules for their selection. According to different criteria, the seismic coefficient should be considered part of peak ground acceleration because soil slopes are not rigid, and the peak acceleration could be generated quickly. Table 4 presents the horizontal seismic coefficient values recommended for the design. In this study, one-half of the peak horizontal acceleration was suggested as an appropriate coefficient for soil slopes.

### 3.6 Topographical effect

It is widely accepted that topography affects seismic loads' amplitude and frequency content. Its effect on the ground shaking has been observed during many previous earthquakes (e.g., 3rd March 1985, Mw 7.8, Chile Earthquake, Loma Prieta Earthquake, Hartzell, et al., 1994; 17th January 1994, Mw 6.9, Northridge Earthquake). There are significant differences between the levels of the anticipated ground motions. Some studies report that amplitudes can increase ten times theoretical estimates [99]. However, the codes did not include technical notes regarding side effects until 1790. Ps-92 of France, EC-8(2000-Draft2002), and Iranian 2800 code are some cases that consider a 2D topographical amplification factor. In the Iranian 2800 code, the topographic amplification factor is equal to 1.4 times in slopes with 30 m height and steeper than 15°. In this study, the topographic amplification factor was selected to be about 1.4.

### 3.7 Peak horizontal acceleration

Overall, 50 accelerographs are recorded in the Manjil-Roudbar earthquake within a radius of 250 km around the earthquake epicenter. The most vigorous ground motion was recorded at Abbar station at about 8 km from the major fault. The maximum horizontal and vertical values were approximately 0.65 and 0.52 g (Fig. 14), respectively.

### 3.8 Lakeh landslide back-analysis

As shown on the landslide inventory map (Fig. 5), 27 landslides have occurred in the study area, most of which are in the soil material at the lower part of the GSI chart where GSI could not be determined using the Hoek–Brown method. Only a limited number of the triggered landslides were situated in the rock mass, capable of overcoming the limitations of the Hoek and Brown criterion. Five landslides were located in the Lakeh region northwest of Roudbar, one of which contained a rotational failure mechanism and was selected for the back-analysis in this study (Fig. S11). The shear strength of the sliding surface was unknown in the back-analysis, while the shape of the landslide was known. The slip mechanism was evident in the selected landslide, whereas the slip surface was unclear. The failure mechanism, critical slip surface, and strength were investigated in the back-analysis. The landslide was about 160 m high, and the slope was 350 m long and 3.7 km far from the major Roudbar-Manjil fault. Due to the coherent nature of the silty sandstone, the rock mass was assumed homogeneous and isotropic. In the back-analysis process, the internal friction angle was assumed constant. The cohesion value was investigated based on the complexity involved in cohesion determination by employing sensitivity analysis to determine the  $c$  value with a constant value of the friction angle. The safety factor is considered equal to unity, which is the rupture threshold.

**Table 4** Recommended horizontal seismic coefficients [43]

| Horizontal Seismic Coefficient ( $k_h$ ) | Description                        |                        |
|--|------------------------------------|------------------------|
| 0.05–0.15                                | In the United States               |                        |
| 0.12–0.25                                | In Japan                           |                        |
| 0.1                                      | “Severe” earthquakes               | Terzaghi [4]           |
| 0.2                                      | “Violent, destructive” earthquakes |                        |
| 0.5                                      | “Catastrophic” earthquakes         |                        |
| 0.1–0.2                                  | Seed [2], FOS 1.15                 |                        |
| 0.10                                     | Major Earthquake, FOS > 1.0        | Corps of Engineers [5] |
| 0.15                                     | Great Earthquake, FOS > 1.0        |                        |
| ½ to a of PHA                            | Marcuson [6], FOS > 1.0            |                        |
| ½ of PHA                                 | Hynes-Griffin [7], FOS > 1.0       |                        |

FOS Factor of safety; PHA Peak horizontal acceleration, in  $g$ 's

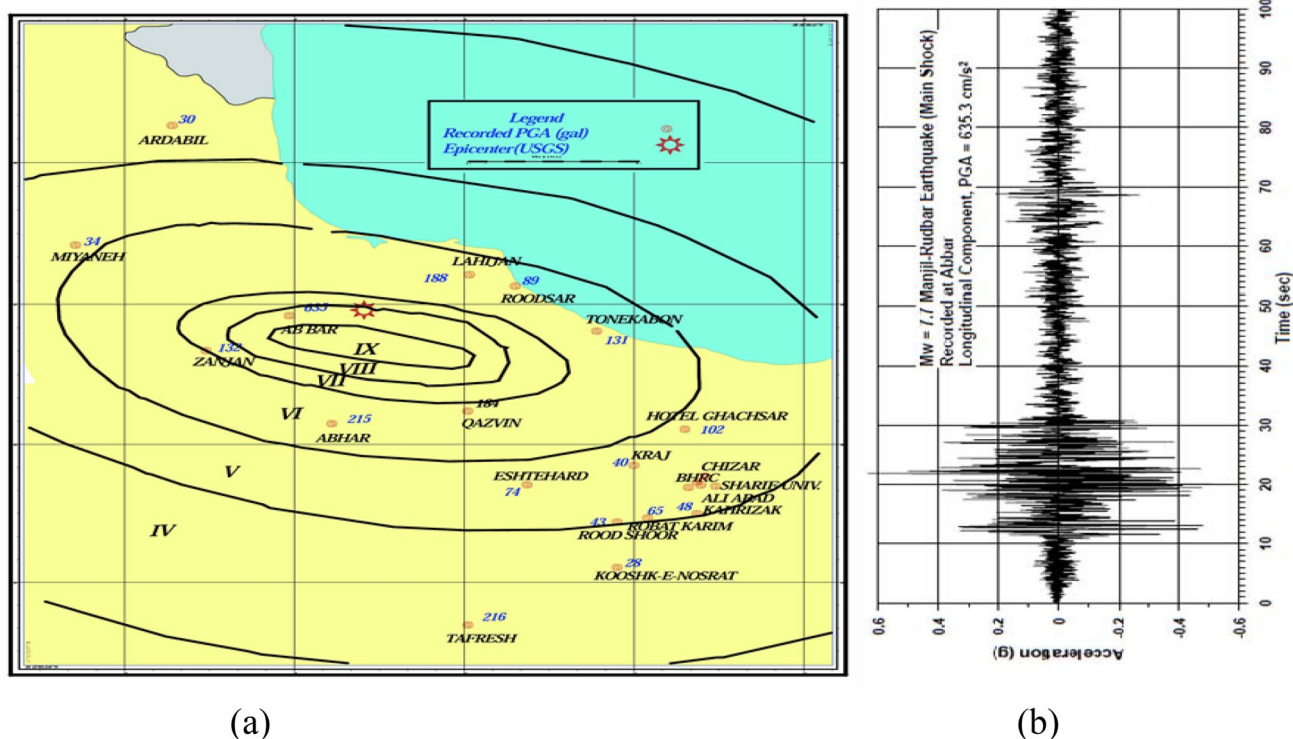


**Fig. 5** Abbar station **a** and horizontal component of the strong motion **b** p recordings of the Manjil-Rudbar earthquake (BHCR)

The average unit weight ( $\gamma$ ) of the heavily broken portion of the silty sandstone was 22 kN/m<sup>3</sup>. Based on Table 4, the average internal friction angle and cohesion values were about 40 and 230 kN/m<sup>2</sup>, respectively. No groundwater table was observed in the slope, and it was kept dry.

SLIDE, version 5.0 was adopted to perform sensitive pseudo-static back-analysis in the case studies. The software was proved to be suitable for limit equilibrium analysis based on Bishop’s simplified method (Bishop, 1955). The maximum horizontal acceleration was also considered to be 0.455 [0.5 \* (1.4\*0.65) = 0.455].

For the sensitive pseudo-static back-analysis,  $\phi = 33$  and a range of  $\pm 20$  kN/m<sup>2</sup> were selected for the maximum and minimum cohesion values. As shown in Fig. 6, the minimum safety factor value was about 1.009, and there was a good compatibility between critical and actual slip surfaces. Based on the sensitivity back-analysis, the cohesion value of the rupture threshold was 221.5 kN/m<sup>2</sup> (Fig. S12).

#### 4 Discussions

Based on the results of the back-analysis, using average lithological shear strength parameters, there was high

compatibility between the slope geometry and location of the sliding surface and the observed slip surface. The shear strength parameters of each lithology were obtained by studying several stations based on the GSI method, and their critical values were considered. The shear strength parameters of the obtained sliding surface from the back-analysis were less than the average shear strength parameters (Table 4). In other words, landslides occur where the shear strength parameters are less than the values resulting from the Hoek–Brown method.

#### 5 Conclusions

In general, assessing the strength parameters of medium-scale geological formations, which thousands of slopes may encounter, could be an essential research topic in slope stability analysis. Seismic-landslide hazard zonation in the regional scale using Newmark’s displacement method and GIS software proved straightforward and applicable. The shear strength parameters of the geological formation were necessary. According to previous studies and field investigation, the earthquake-induced landslide inventory map of the region in the Roudbar-Manjil Earthquake was prepared. In general, 27



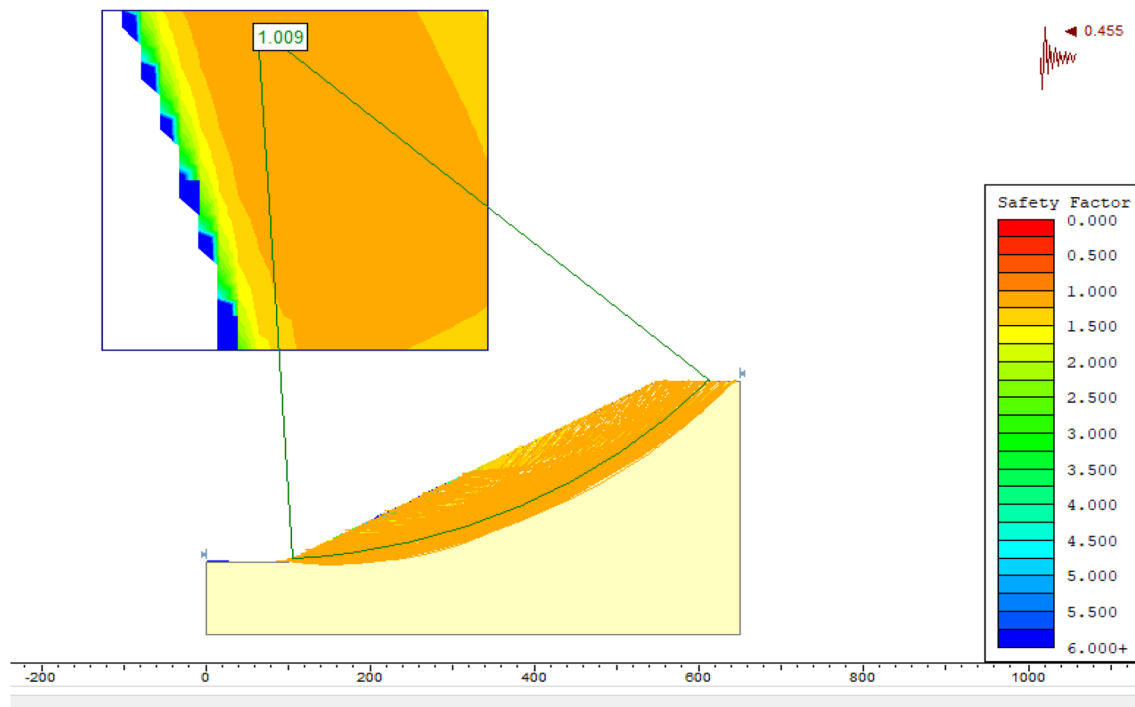


**Fig. 6** Limit equilibrium model provided for the back-analysis of Lakeh landslide

recognized landslides were found and mapped after comparing these studies. The shear strength parameters in the Roudbar quadrangle as a high-risk landslide area were determined using several sources. The GSI classification system was employed to obtain the GSI of 400 points in all formations. The shear strength parameters were determined by this method, compiled shear data, and experienced geological engineers. The average values of the shear strength parameters of the sources were assigned as the constraints, according to which all slopes were considered statically stable. Moisture content was calculated using the NDMI. Finally, the required shear strength parameters for the stability of the computer model were obtained, followed by obtaining and comparing the shear strength parameters of all formations with those of other studies. These parameters were near the average values of the shear strength data. The data were used to analyze seismic-landslide hazard zonation, emergency response efforts, and public information through the media.

## References

- Fathizad, H., Tazeh, M., Kalantari, S., & Shojaei, S. (2017). The investigation of spatiotemporal variations of land surface temperature based on land use changes using NDVI in southwest of Iran. *Journal of African Earth Sciences*, *134*, 249–256.
- Nhu, V. H., Rahmati, O., Falah, F., Shojaei, S., Al-Ansari, N., Shahabi, H., Shirzadi, A., Górski, K., Nguyen, H., & Ahmad, B. B. (2020). Mapping of groundwater spring potential in karst aquifer system using novel ensemble bivariate and multivariate models. *Water*, *12*(4), 985.
- Khanamani, A., Fathizad, H., Karimi, H., & Shojaei, S. (2017). Assessing desertification by using soil indices. *Arabian Journal of Geosciences*, *10*(13), 1–10.
- Arabi Aliabad, F., Shojaei, S., Zare, M., & Ekhtesasi, M. R. (2019). Assessment of the fuzzy ARTMAP neural network method performance in geological mapping using satellite images and Boolean logic. *International Journal of Environmental Science and Technology*, *16*(7), 3829–3838.
- Alipur, H., Zare, M., & Shojaei, S. (2016). Assessing the degradation of vegetation of arid zones using FAO–UNIP model (case study: Kashan zone). *Modeling Earth Systems and Environment*, *2*(4), 1–6.
- Shojaei, S., Ardakani, M. A. H., & Sodaiezhadeh, H. (2019). Optimization of parameters affecting organic mulch test to control erosion. *Journal of Environmental Management*, *249*, 109414.
- Shano, L., Raghuvanshi, T. K., & Meten, M. (2020). Landslide susceptibility evaluation and hazard zonation techniques—a review. *Geoenvironmental Disasters*, *7*(1), 1–19.
- Piri, I., Moosavi, M., Taheri, A. Z., Alipur, H., Shojaei, S., & Mousavi, S. A. (2019). The spatial assessment of suitable areas for medicinal species of *Astragalus* (*Astragalus hypsogeton* Bunge) using the Analytic Hierarchy Process (AHP) and Geographic Information System (GIS). *The Egyptian Journal of Remote Sensing and Space Science*, *22*(2), 193–201.
- Shojaei, S., Alipur, H., Ardakani, A. H. H., Nasab, S. N. H., & Khosravi, H. (2018). Locating *Astragalus hypsogeton* Bunge appropriate site using AHP and GIS. *Spatial Information Research*, *26*(2), 223–231.
- Shojaei, S., Shojaei, S., & Sasani, M. (2017). The efficiency of eliminating Direct Red 81 by Zero-valent Iron nanoparticles from

- aqueous solutions using response surface Model (RSM). *Modeling Earth Systems and Environment*, 3(1), 1–7.
11. Dehghani, A. A., Bahremand, A. R., & Shojaei, S. (2017). Intelligent estimation of flood hydrographs using an adaptive neuro-fuzzy inference system (ANFIS). *Modeling Earth Systems and Environment*, 3(1), 1–9.
  12. Cheshmidari, M. N., Hatefi Ardakani, A. H., Alipor, H., & Shojaei, S. (2017). Applying Delphi method in prioritizing intensity of flooding in Ivar watershed in Iran. *Spatial Information Research*, 25(2), 173–179.
  13. Piri, I., Khanamani, A., Shojaei, S., & Fathizad, H. (2017). Determination of the best geostatistical method for climatic zoning in Iran. *Applied Ecology and Environmental Research*, 15(1), 93–103.
  14. Hamidy, N., Alipur, H., Nasab, S. N. H., Yazdani, A., & Shojaei, S. (2016). Spatial evaluation of appropriate areas to collect runoff using Analytic Hierarchy Process (AHP) and Geographical Information System (GIS)(case study: The catchment “Kasef” in Bardaskan. *Modeling Earth Systems and Environment*, 2(4), 1–11.
  15. Shojaei, S., Ardakani, M. A. H., & Sodaiezhadeh, H. (2020). Simultaneous optimization of parameters influencing organic mulch test using response surface methodology. *Scientific reports*, 10(1), 1–11.
  16. Rastegaripour, F., Saboni, M. S., Shojaei, S., & Tavassoli, A. (2019). Simultaneous management of water and wastewater using ant and artificial neural network (ANN) algorithms. *International Journal of Environmental Science and Technology*, 16(10), 5835–5856.
  17. Eslami, Z., Shojaei, S., & Hakimzadeh, M. A. (2017). Exploring prioritized sub-basins in terms of flooding risk using HEC\_HMS model in Eskandari catchment. *Iran. Spatial Information Research*, 25(5), 677–684.
  18. Aliabad, F. A., & Shojaei, S. (2019). The impact of drought and decline in groundwater levels on the spread of sand dunes in the plain in Iran. *Sustainable Water Resources Management*, 5(2), 541–555.
  19. Shojaei, S., Jafarpour, A., Shojaei, S., Gyasi-Agyei, Y., & Rodrigo-Comino, J. (2021). Heavy metal uptake by plants from wastewater of different pulp concentrations and contaminated soils. *Journal of Cleaner Production*, 296, 126345.
  20. Shojaei, S., Kalantari, Z., & Rodrigo-Comino, J. (2020). Prediction of factors affecting activation of soil erosion by mathematical modeling at pedon scale under laboratory conditions. *Scientific Reports*, 10(1), 1–12.
  21. Ardakani, A. H. H., Shojaei, S., Siasar, H., & Ekhtesasi, M. R. (2020). Heuristic evaluation of groundwater in arid zones using remote sensing and geographic information system. *International Journal of Environmental Science and Technology*, 17(2), 633–644.
  22. Malamiri, H. R. G., Aliabad, F. A., Shojaei, S., Morad, M., & Band, S. S. (2021). A study on the use of UAV images to improve the separation accuracy of agricultural land areas. *Computers and Electronics in Agriculture*, 184, 106079.
  23. Shojaei, S., Shojaei, S., Nouri, A., & Baharinikoo, L. (2021). Application of chemometrics for modeling and optimization of ultrasound-assisted dispersive liquid–liquid microextraction for the simultaneous determination of dyes. *npj Clean Water*, 4(1), 1–8.
  24. Dou, J., Yamagishi, H., Pourghasemi, H. R., Yunus, A. P., Song, X., Xu, Y., & Zhu, Z. (2015). An integrated artificial neural network model for the landslide susceptibility assessment of Osado Island, Japan. *Natural Hazards*, 78(3), 1749–1776.
  25. Hong, H., Pradhan, B., Xu, C., & Bui, D. T. (2015). Spatial prediction of landslide hazard at the Yihuang area (China) using two-class kernel logistic regression, alternating decision tree and support vector machines. *CATENA*, 133, 266–281.
  26. Zhang, T., Han, L., Chen, W., & Shahabi, H. (2018). Hybrid integration approach of entropy with logistic regression and support vector machine for landslide susceptibility modeling. *Entropy*, 20(11), 884.
  27. Shojaei, S., Ardakani, M. A. H., Sodaiezhadeh, H., Jafari, M., & Afzali, S. F. (2019). Optimization using response surface method (RSM) to investigate the compaction of mulch. *Modeling Earth Systems and Environment*, 5(4), 1553–1561.
  28. Forozan, G., Elmi, M. R., Talebi, A., Mokhtari, M. H., & Shojaei, S. (2020). Temporal-spatial simulation of landscape variations using combined model of markov chain and automated cell. *KN-Journal of Cartography and Geographic Information*, 70(2), 45–53.
  29. Jibson, R. W., Harp, E. L., & Michael, J. A. (2000). A method for producing digital probabilistic seismic landslide hazard maps. *Engineering Geology*, 58(3–4), 271–289.
  30. Sarma, S. K. (1981). Seismic displacement analysis of earth dams. *Journal of Geotechnical and Geoenvironmental Engineering*, 107(12), 1735–1739.
  31. Wilson, R. C., & Keefer, D. K. (1983). Dynamic analysis of a slope failure from the 6 August 1979 Coyote Lake, California, earthquake. *Bulletin of the Seismological Society of America*, 73(3), 863–877.
  32. Jibson, R. W. (1993). Predicting earthquake-induced landslide displacements using Newmark’s sliding block analysis. *Transportation Research Record*, 1411, 9–17.
  33. Fathizad, H., Pakbaz, N., Sodaiezhadeh, H., & Shojaei, S. (2017). Exploring canola planting area using AHP associated with GIS in Meymeh-Zarinabad of Iran. *Spatial Information Research*, 25(3), 371–379.
  34. Poudineh, Z., Fakheri, B. A., Sirosmehr, A. R., & Shojaei, S. (2018). Genetic and morphological diversity of fennel by using ISSR marker and biplot analysis. *Indian Journal of Plant Physiology*, 23(3), 564–572.
  35. Shojaei, S., Ardakani, M. A. H., Sodaiezhadeh, H., Jafari, M., & Afzali, S. F. (2021). New laboratory techniques (novel) in making organic-mineral mulch to control wind and water erosion and its use in global scale. *Spatial Information Research*, 29(1), 97–107.
  36. Marinou, P., & Hoek, E. (2000). GSI: A geologically friendly tool for rock mass strength estimation. In *Proceedings of the Geo-Eng2000 at the international conference on geotechnical and geological engineering* (pp. 1422–1446). Melbourne, Lancaster: Technomic publishers.
  37. Saygili, G., & Rathje, E. M. (2008). Empirical predictive models for earthquake-induced sliding displacements of slopes. *Journal of Geotechnical and Geoenvironmental Engineering*, 134(6), 790–803.
  38. Bakhtiyari, E., Almasi, A., Cheshomi, A., & Hassanpour, J. (2017). Determination of shear strength parameters of rock mass using back analysis methods and comparison of results with empirical methods. *European Journal of Engineering Research and Science*, 2(11), 35–42.
  39. Ng, S. M., Ismail, M. A., & Abustan, I. (2014). Back analysis of slope failure using finite element with point estimate method (FEM-PEM). *Journal of Civil Engineering Research*, 4(3A), 31–35.
  40. Hoek, E., & Brown, E. T. (1997). Practical estimates of rock mass strength. *International Journal of Rock Mechanics and Mining Sciences*, 34(8), 1165–1186.
  41. Akin, M. (2013). Slope stability problems and back analysis in heavily jointed rock mass: A case study from Manisa, Turkey. *Rock Mechanics and Rock Engineering*, 46(2), 359–371.
  42. Marinou, V., Fortsakis, P., & Proutzopoulos, G. (2006). Estimation of rock mass properties of heavily sheared flysch using data from tunnelling construction. IAEG2006, paper. 2006(314).

43. MahdaviFar, M., & Memarian, P. (2013). Assessment of earthquake-induced landslides triggered by Roudbar-Manjil earthquake in Rostamabad (Iran) quadrangle using knowledge-based hazard analysis approach. *earthquake-induced landslides* (pp. 769–780). Berlin, Heidelberg: Springer.
44. MahdaviFar, M. R. (2006). Analytical evaluation and design of landslide risk management system of the earthquake in Iran. PhD thesis, IIEES (International Institute of Earthquake Engineering and Seismology).
45. Zare, M. (2005). Introduction to Applied Seismology, IIEES (International Institute of Earthquake Engineering and Seismology).
46. Harp, E. L., Jibson, R. W., & Dart, R. L. (2013). The effect of complex fault rupture on the distribution of landslides triggered by the 12 January 2010, Haiti earthquake. *Landslide Science and Practice 2013* (pp. 157–161). Berlin, Heidelberg: Springer.
47. Khaksari, M., (2013). Landslide hazard zonation of earthquake ROODBAR with two methods to shape the quality and quantity of Rostam Abad, M. S thesis, Islamic Azad University, Science and Research.
48. Guzzetti, F., Mondini, A. C., Cardinali, M., Fiorucci, F., Santangelo, M., & Chang, K. T. (2012). Landslide inventory maps: New tools for an old problem. *Earth-Science Reviews*, *112*(1–2), 42–66.
49. Hoek, E. (1994). Strength of rock and rock masse. 4–16.
50. Hoek, T. L. V., Li, C., Shao, Z., Schumacker, P. T., & Becker, L. B. (1997). Significant levels of oxidants are generated by isolated cardiomyocytes during ischemia prior to reperfusion. *Journal of Molecular and Cellular Cardiology*, *29*(9), 2571–2583.
51. Jibson, R. W. (2007). Regression models for estimating coseismic landslide displacement. *Engineering Geology*, *91*(2–4), 209–218.
52. Keefer, D. K. (1984). Landslides caused by earthquakes. *Geological Society of America Bulletin*, *95*(4), 406–421.

**Publisher's Note** Springer Nature remains neutral with regard to jurisdictional claims in published maps and institutional affiliations.